Vol. 29 • No. 3 • January 17 • 2019

www.afm-journal.de

ADVANCED FUNCTIONAL MATERIALS

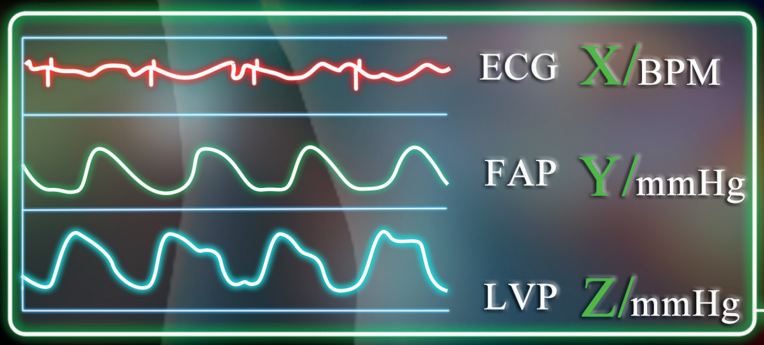

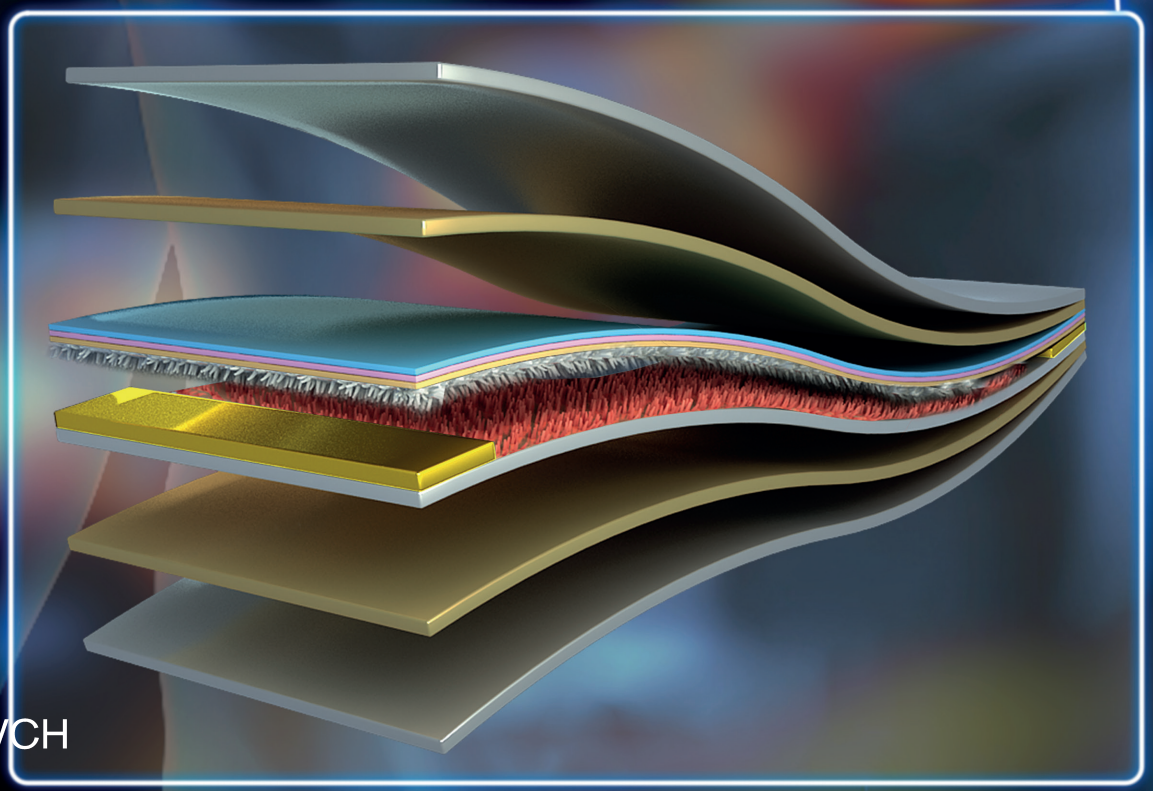

WILEY-VCH

Transcatheter Self-Powered Ultrasensitive Endocardial Pressure Sensor

Zhuo Liu, Ye Ma, Han Ouyang, Bojing Shi, Ning Li, Dongjie Jiang, Feng Xie, Dan Qu, Yang Zou, Yue Huang, Hu Li, Chaochao Zhao, Puchuan Tan, Min Yu, Yubo Fan, Hao Zhang,* Zhong Lin Wang,* and Zhou Li**

Changes in endocardial pressure (EP) have important clinical significance for heart failure patients with impaired cardiac function. As a vital parameter for evaluating cardiac function, EP is commonly monitored by invasive and expensive cardiac catheterization, which is not feasible for long-term and continuous data collection. In this work, a miniaturized, flexible, and self-powered endocardial pressure sensor (SEPS) based on triboelectric nanogenerator (TENG), which is integrated with a surgical catheter for minimally invasive implantation, is reported. In a porcine model, SEPS is implanted into the left ventricle and the left atrium. The SEPS has a good response both in low- and high-pressure environments. The SEPS achieves the ultrasensitivity, real-time monitoring, and mechanical stability in vivo. An excellent linearity (R^2 = 0.997) with a sensitivity of 1.195 mV mmHg^{-1} is obtained. Furthermore, cardiac arrhythmias such as ventricular fibrillation and ventricular premature contraction can also be detected by SEPS. The device may promote the development of miniature implantable medical sensors for monitoring and diagnosis of cardiovascular diseases.

1. Introduction

Heart failure (HF) is a global public health problem in which the heart is incapable to pump sufficient blood to meet the body's needs.[1] Typical symptoms of HF include dyspnea, weakness, fatigue and edema of lower extremities, which cause poor quality of life, high mortality and heavy economic burden associated with HF diagnosis and treatment.[2] A crucial indicator of the heart's ability to pump blood and the effects of therapeutic approaches is endocardial pressure (EP), such as atrial and ventricular pressure. As the only effective approach in clinical practice to obtain EP data,[3] cardiac catheterization is expensive, invasive and not feasible for long-term and continuous data collection. In addition, an external bulky recorder connected with cardiac catheterization will also bring a series of short boards, such as complex operation and inadequate compliance to patients. In clinical practice, the intermittent measurement of EP will cause negligence of transient/silent symptoms, which may result in misdiagnosis of patients. In 2002, Brockway and Doten have proposed a patent about long-term monitoring EP by integrating a remote sensor, a telemetry unit and a pressure transmission catheter.[4] However, experimental or clinical study of

Z. Liu, Dr. B. Shi, H. Li, Prof. Y. Fan
Beijing Advanced Innovation Centre for Biomedical Engineering
Key Laboratory for Biomechanics and Mechanobiology
of Chinese Education Ministry
School of Biological Science and Medical Engineering
Beihang University
Beijing 10083, China
E-mail: yubofan@buaa.edu.cn

Z. Liu, Dr. B. Shi, H. Li, Prof. Y. Fan
Beijing Key Laboratory for Design and Evaluation Technology
of Advanced Implantable & Interventional Medical Devices
Beihang University
Beijing 10083, China

Dr. Y. Ma, N. Li, F. Xie, D. Qu, Y. Huang, Prof. H. Zhang
Institute of Cardiothoracic Surgery at Changhai Hospital
Second Military Medical University
Shanghai 200433, China
E-mail: zhanghao@smmu.edu.cn

The ORCID identification number(s) for the author(s) of this article can be found under https://doi.org/10.1002/adfm.201807560.

H. Ouyang, D. Jiang, Y. Zou, C. Zhao, P. Tan, Dr. M. Yu, Prof. H. Zhang, Prof. Z. L. Wang, Prof. Z. Li
CAS Center for Excellence in Nanoscience
Beijing Key Laboratory of Micro-nano Energy and Sensor
Beijing Institute of Nanoenergy and Nanosystems
Chinese Academy of Sciences
Beijing 100083, China;
E-mail: zhong.wang@mse.gatech.edu; zli@binn.cas.cn

H. Ouyang, D. Jiang, Y. Zou, C. Zhao, P. Tan, Dr. M. Yu, Prof. Z. Li
College of Nanoscience and Technology
University of Chinese Academy of Sciences
Beijing 100049, China

Prof. Y. Fan
National Research Center for Rehabilitation Technical Aids
Beijing 100176, China

Prof. Z. L. Wang
School of Materials Science and Engineering
Georgia Institute of Technology
Atlanta, GA 30332, USA

DOI: 10.1002/adfm.201807560

this EP sensory system has not been reported. Developing a real-time, high-sensitivity and low-cost sensor to monitor EP is significantly important and urgent.

Synergistic development of advanced materials/electronic and nanotechnology will promote progress in medical monitoring and application.[5] Recently, nanogenerators (NGs) have been demonstrated for successfully scavenging and converting mechanical energy into electric power based on piezoelectric and triboelectric effects.[6] The fabrication techniques and associated unusual device structures are helping to advance application of NGs within the human body.[7,8] Moreover, previous reports proved that abundant physiological and biomedical information in the electrical outputs of NGs, such as heart rate, pulse and respiration.[9,10] Moreover, NG technology utilizing human body motions and organ activities as the energy source can realize self-powered healthcare systems and active sensors.[11] There are some favorable advantages of those devices including high sensitivity, ultraflexibility and easy readout feature.[12] Compared with current devices, smaller physiological signal sensors based on NGs with characteristics of higher outputs, ultrasensitivity and excellent biocompatibility appear to be more critical. It will broaden the application scenarios of the NG-based sensors, and more in-depth physiological signals can be acquired in a minimally invasive surgical approach .

Here, we proposed a miniaturized, flexible, ultrasensitive and self-powered endocardial pressure sensor (SEPS) for real-time EP monitoring. SEPS is based on triboelectric nanogenerator (TENG), which can convert the energy of blood flow within the heart chambers into electricity. The electric outputs of the device can indicate physiological and pathological cardiovascular status, including EP, ventricular fibrillation and ventricular premature contraction. The SEPS was flexible and miniaturized enough to be implanted into the heart by minimally invasive surgery. Meanwhile, the in vitro and in vivo sensory capabilities were both studied. An excellent linearity ($R^2 = 0.997$) with a sensitivity of 1.195 mV $mmHg^{-1}$ was obtained. In vitro results demonstrated the mechanical and electrical stability of the device by swinging over 100 million cycles in a humid environment. Additional results showed an excellent blood compatibility of the encapsulation layer with sufficiently low risks of arousing hemolytic reaction and activating the coagulation cascade. Furthermore, based on the changes in EP, cardiac arrhythmias such as ventricular fibrillation and ventricular premature contraction can also be detected. These developments can help safely sense pressure situation, diagnose and monitor cardiovascular disease, which shows a promising perspective in the field of implantable health care monitoring.

2. Results and Discussion

To achieve more ideal leak-proofness, superior sensitivity and flexibility, the multilayered structure was introduced to fabricate the SEPS, which consisted of the encapsulation layers, electrode layers, triboelectric layers and spacer layers. The SEPS in bending and original states displayed great flexibility and deformation-recovery ability (**Figure 1**a). The overall size of the device was 1 cm × 1.5 cm × 0.1 cm. Schematic illustration of the SEPS is shown in Figure 1b. The surface of the nano-polytetrafluoroethylene (PTFE) film was treated by the inductively coupled plasma (ICP) method.[13] Scanning electron micrograph (SEM) and atomic force microscope (AFM) images of the nano-PTFE film (25 μm) employed as one of the triboelectric layers are shown in Figure 1c,d, respectively. An ultrathin gold (Au) layer (50 nm) was deposited on the back of the nano-PTFE film to act as one of the electrodes. A kapton film (150 μm) was fixed on the nano-PTFE layer, served as a flexible substrate. An Al foil (100 μm) acted as both the other triboelectric layer and electrode. A 3D ethylene-vinyl acetate (EVA) copolymer film (500 μm) was employed as the spacer layer. It was placed between the two triboelectric layers to further guarantee the effective contact and separation process. To further promote the output performance and sensitivity of the SEPS,[14] a method of corona discharge was employed to modify the surface of nano-PTFE, which achieved higher surface charge density (Figure 1e).

The detailed operating principle of the SEPS based on the coupling of contact electrification and electrostatic induction is illustrated in Figure 1f. In brief, at original state, no charge is generated or inducted on both surfaces of the triboelectric layers. When the SEPS is pressed, the nano-PTFE layer is brought into vertical contact with the Al layer, while electrons are injected from the Al layer into nano-PTFE due to the difference in triboelectric series, leading to net positive charges at Al layer and net negative charges at nano-PTFE layer. As the SEPS starts to be released, the nano-PTFE film intends to revert back to its original position due to its own resilience. Once the two layers separate, an electric potential difference is then established between the two electrodes. Specifically, fluctuations of the EP can cause a separating and contacting process between the two triboelectric layers, resulting in a periodically changing voltage on the external circuit. If the electric potential of the Al electrode (U_A) is defined as zero, that of the Au electrode (U_G) can be calculated by

$$U_G = -\frac{\sigma d'}{\varepsilon_0} \tag{1}$$

where σ is the triboelectric charge density, d' is the distance between two triboelectric layers, and ε_0 is the vacuum permittivity.

Therefore, as the SEPS is released, the output open-circuit voltage (V_{oc}) will keep increasing till reaching the maximal value when the nano-PTFE film fully reverts to the original position. Such a signal will remain constant, provided that the input impedance of the electrometer is infinitely large. If pressing is immediately followed, the electric potential difference starts diminishing during the process of the two triboelectric layers getting closer to each other. As a result, V_{oc} will drop from the maximal value to zero when a full contact appears again between the two layers. Along with the dilating and contracting of the heart, cyclic electric output signals can be detected.

We systematically investigated the effect of the corona discharge process on the output performance of SEPS in vitro by applying a periodic external mechanical force. The V_{oc} of the SEPS before corona discharge could reach ≈1.2 V (**Figure 2**a). After the corona discharge process, the average values of V_{oc} of the SEPS was elevated to ≈6.2 V (Figure 2b). The statistical comparison of the average V_{oc} of the SEPS

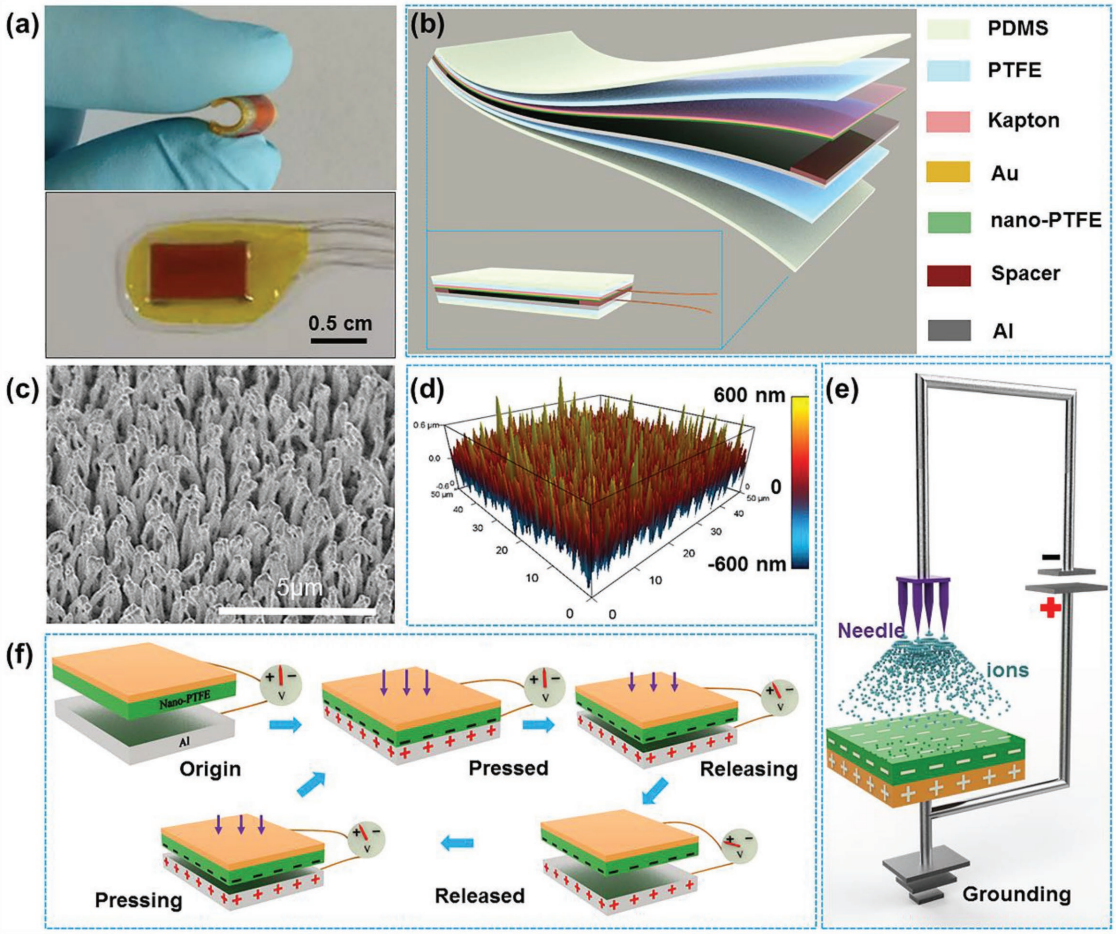

Figure 1. a) Photograph of the SEPS in bending and original states. b) Schematic illustration of the structure of the SEPS. c) SEM image of a nanostructure on the PTFE film. d) AFM image of a nanostructure on the PTFE film. e) Schematic illustration of a corona discharge system. f) Schematic proposed mechanisms of the device working in a vertical contact-separation mode.

before and after corona discharge is shown in Figure 2c. With the corona discharge process, the V_{oc} of the SEPS was enhanced by fivefold.

Mechanical robustness needs to be assessed for long-term application in in vivo environment with circumferential extrusion and moisture. Photographs of the fatigue testing system and the SEPS at different cycle numbers are shown in Figure 2d. The SEPS was immersed in normal saline to simulate the body environment. The frequency applied in the fatigue test was 100 Hz. Every 20 million times, the performance of the SEPS was tested. After 100 million working cycles, the V_{oc} of the SEPS (Figure 2e) maintained stable in comparison with its initial state, exhibiting an outstanding durability.

Beside in vivo integrity and reliability of the device in atrioventricular cavities filled with blood, an acceptable blood compatibility is also required for the encapsulation layers. When blood flow encounters an artificial surface, a complex series of interacting events will occur, which may result in hemolytic or clotting reactions. Therefore, hemolysis and coagulation on the encapsulation layers were also characterized. The average hemolysis rate of the encapsulation layers was 1.08%, which was remarkably lower than the international standards organization (ISO) standard (5%) and would not induce the hemolytic reaction inside the body (Figure 2f). The red blood cells (RBCs) maintained a good cell morphology after contacting with the encapsulation layers (Figure 2g). The SEM images of positive and negative control groups are shown in Figure S1 (Supporting Information).

The adherence and morphology of platelets on encapsulation layers under different magnification were also examined by SEM. Figure 2h typically shows the encapsulation layers without adhesion of red blood cell or fibrin formation. There were very few adhered platelets sporadically distributed on the surface of the encapsulating materials. Almost all platelets adherent to the surface of the encapsulation layer retained their round morphology and there was no apparent deformation, agglomeration and pseudopod formation, indicating a less activated status. Collectively, the results demonstrated an excellent blood compatibility of the encapsulation layer with sufficiently low risks of arousing hemolytic reactions and activating the coagulation cascade.

The outputs of the SEPS were originated from external forces and might carry abundant information about its received circumferential force. Therefore, we examined the sensory

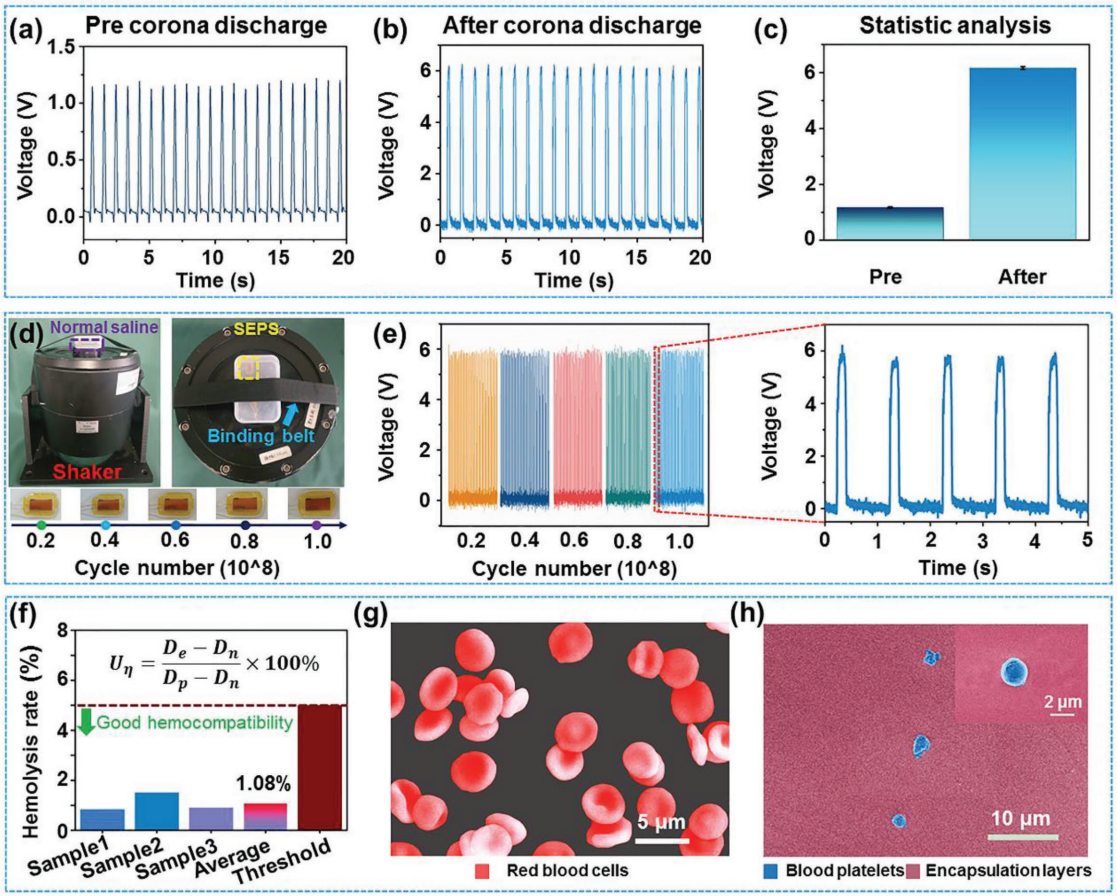

Figure 2. a) V_{oc} of SEPS before corona discharge. b) V_{oc} of SEPS after corona discharge. c) Statistical comparison of average V_{oc} of the SEPS before and after corona discharge. d) Photographs of the fatigue testing system and the SEPS at different cycles. e) V_{oc} of SEPS and its durability test. f) Hemolysis rate of the encapsulation layer. g) SEM image of red blood cells after contact with the encapsulation layer. h) SEM image of independent platelet adhesion on the encapsulation layer.

functionality and pressure responsiveness of SEPS by performing in vitro experimental evaluations. The set-up of the in vitro testing system is illustrated in **Figure 3**a and Video S1 (Supporting Information), which consists of a gas control unit and a confined chamber to mimic the EP changes. The internal pressure of the confined chamber was monitored by a commercialized probe and displayed using a data acquisition (DAQ) system. The SEPS was immersed in the normal saline inside the confined chamber, and two leads of the device were connected to an electrometer. With the pressure in the confined chamber regulated by the gas control unit, the signals of the SEPS was collected and compared with the data documented by the DAQ system as a reference standard.

The V_{oc} values of the SEPS at different levels of pressure are shown in Figure 3b. We first noticed that the electric outputs of the SEPS increased correspondingly along with the elevating trend of applied pressure ranging from 70 to 350 mmHg (1 mmHg is approximately equal to 133 Pa), yielding higher outputs under a larger pressure. To further inspect and confirm their relationship, correlation analysis and linear fitting were conducted between average values of SEPS output peaks and external pressures. The sensitivity K can be defined as the slope of the peak voltage versus the peak pressure. As shown in the inset of Figure 3b, an excellent linearity ($R^2 > 0.99$) was achieved with a high sensitivity of 1.200 mV mmHg^{-1}.

The signal waveforms of the SEPS and sensing probe were scrutinized in Figure 3c. A corresponding video of our testing system working in vitro is presented in supplement materials. Specifically, we found that the output voltage waves of the SEPS exhibited an exactly similar tendency of variation to the pressure signals acquired by the DAQ system. The overall linearity of the two signal waveforms inside one typical cycle was further investigated. An excellent linearity ($R^2 = 0.997$) with a sensitivity of 1.195 mV mmHg^{-1} was obtained inside one cycle of pressure fluctuating from 0 to ≈350 mmHg (Figure 3c). This result demonstrated that the device has an outstanding sensitivity for pressure monitoring and can maintain an excellent sensory function in a wide pressure range. We further documented the electric output signals of SEPS under a maximal pressure of 350 mmHg (Figure 3d). The V_{oc}, short-circuit current (I_{sc}), and transferred charge (Q_{tc}) were typically about 0.45 V, 0.2 μA, and 0.16 nC, respectively. It is noteworthy that the pressure values we set in in vitro measurements greatly surpassed the endocardial pressure (less than 250 mmHg),[15] suggesting the capability of our device for endocardial pressure monitoring.

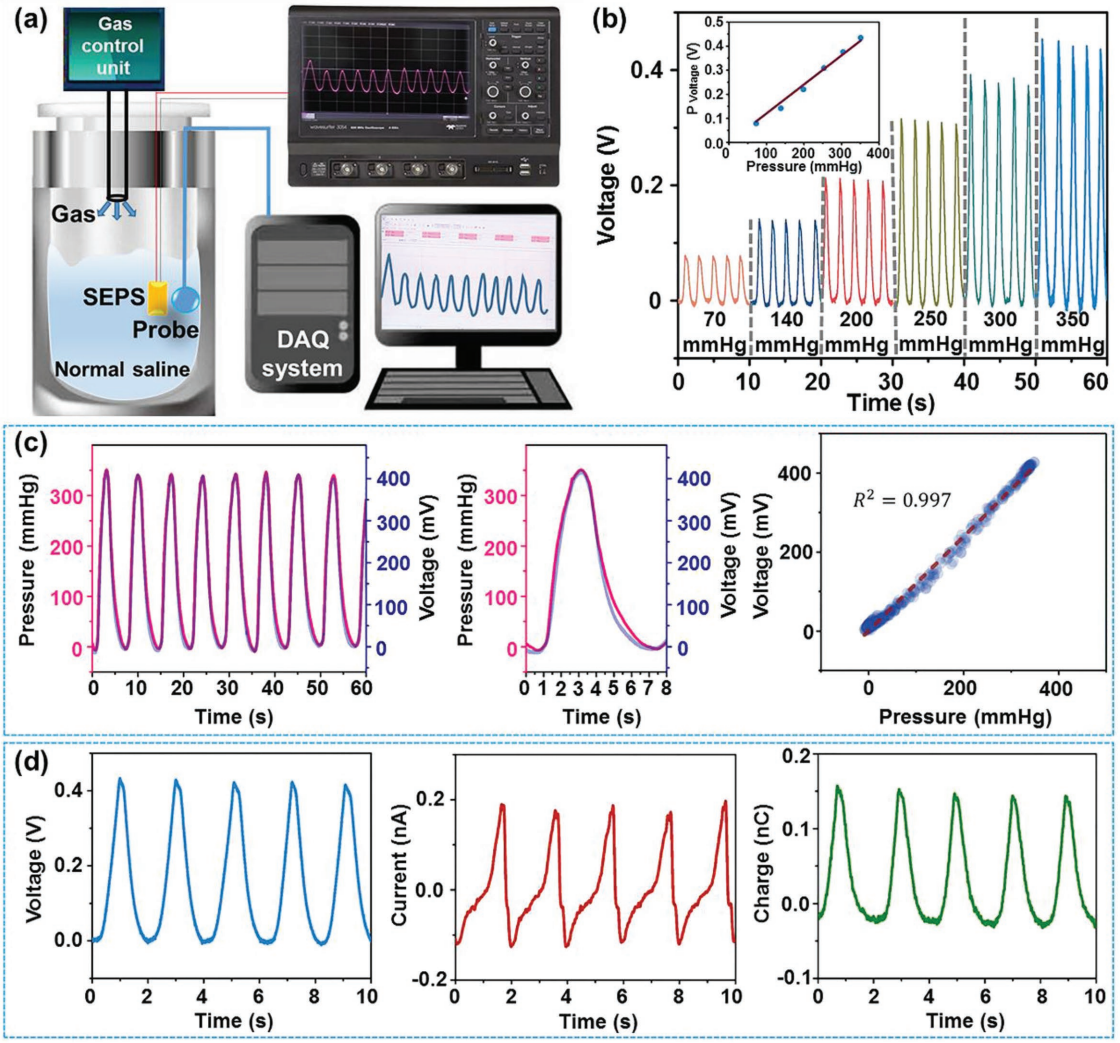

Figure 3. a) Schematic diagram of a system to simulate pressure changes. b) V_{oc} of the SEPS at different pressure levels (inset: the measured results and linear fits of the peak V_{oc} of the SEPS with corresponding pressure peaks). c) Comparison between the waveforms of the pressures and the output voltages of the device with a magnified view of the two waveforms within one typical cycle in the middle (right: The overall linearity of the two signal waveforms inside one typical cycle). d) V_{oc}, I_{sc}, and Q_{tc} of the SEPS at a maximal pressure of 350 mmHg.

To imitatively evaluate the function of the SEPS for real-time biomedical monitoring in human bodies, we selected male adult Yorkshire pigs (40 kg) as our animal model. Before implantation of the SEPS, the animals were intubated and anesthetized by propofol (see the Experimental Section). The signals of electrocardiography (ECG), femoral arterial pressure (FAP), and the SEPS were detected by the DAQ system. The schematic illustration of the in vivo testing system is presented in **Figure 4**a. To achieve minimally invasive implantation, we fabricated a delivery system by integrating the miniature SEPS with a heparin-coated polyvinyl chloride (PVC) stretchable catheter, which is widely used in cardiopulmonary bypass surgery (Figure 4b). In comparison with traditional implantation approaches that involved a 20 cm long skin incision and median sternotomy, a very smaller 2 cm incision of the skin was sufficient for implantation in this study and concomitant iatrogenic orthopedic injury was negligible. The computed tomography (CT) images of SEPS are shown in Figure S2 (Supporting Information). The $BaSO_4$ was mixed with the encapsulation material as a developer, which is only for displaying the position of the SEPS device in the heart more intuitively. The SEPS was implanted into the swine's left ventricle (Video S2, Supporting Information) and a digital radiography (DR) image of the device-implanted heart is shown in Figure 4b.

After implanting the SEPS into the left ventricle, the swine's heart beat normally and the normal vital signs were maintained. The cardiac cycle (alternative occurrence of systolic and diastolic phases) can be roughly divided into five periods, including isovolumetric contraction, rapid ejection, reduced ejection, isovolumetric relaxation and ventricular filling. Each period corresponds to a different value of LVP (Figure S3, Supporting Information). The electric outputs of SEPS are generated from periodic changes in ventricular pressure as a result of cardiac contraction and relaxation, and thus carried abundant information about physiological parameters.

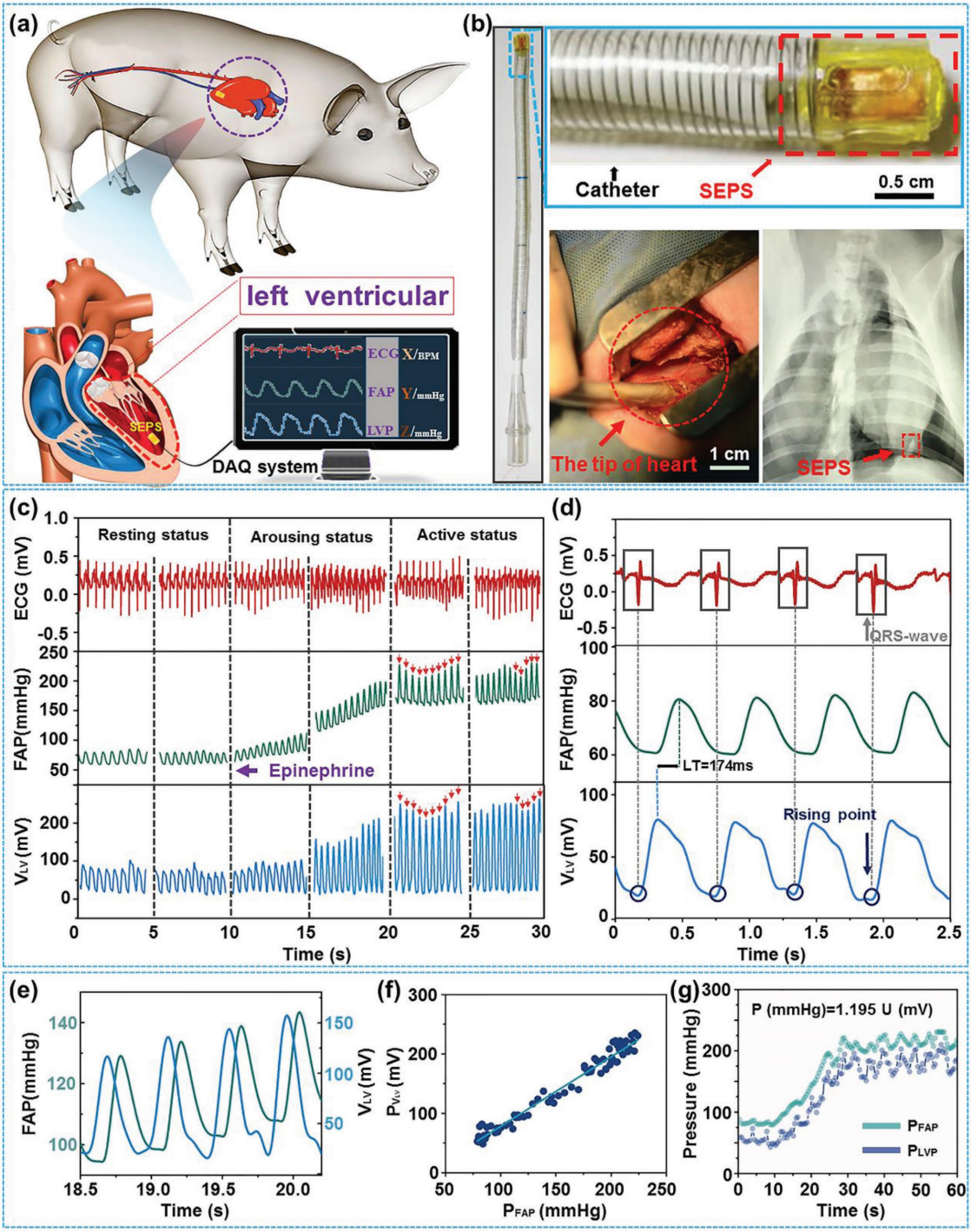

Figure 4. a) Schematic diagram of the semaphore acquisition from the SEPS implanted into an Adult Yorkshire swine's heart. b) Photograph of minimally invasive surgery with a DR image of the heart implanted a device by integration with a surgical delivery system. c) The comparison of working signals from the ECG, FAP and SEPS under different physical status. d) QRS waves of ECG (rectangles) absolutely corresponded to the rising points of the SEPS outputs (circles), and the leading time (LT) represents the time interval between the peaks of the two corresponding waveforms (SEPS and FAP). e) Outputs of the SEPS increased along with the FAP under arousing status. f) Linear correlation between peak V_{oc} of the SEPS and peak FAP. g) Real-time comparison between pressure peaks derived from FAP and SEPS based on $K = 1.195$ mV mmHg^{-1}.

Working signals of ECG, FAP, and SEPS were documented and compared under resting, arousing and active conditions, as exhibited in Figure 4c. At the resting status (systolic FAP < 100 mmHg), a positive V_{oc} of ≈80 mV was obtained, with both FAP and V_{oc} remaining constant, indicating that the miniature and flexible device exerted little interruption on the stableness of cardiac functionality. To further investigate the responsiveness of SEPS to the changes of endocardial pressure,

a natural hormone (epinephrine) secreted during exercise and can enhance cardiac contractility, was introduced to step up the pressure. Along with the elevation of systolic FAP from ≈90 to ≈180 mmHg as a result of epinephrine injection, the peak V_{oc} of the SEPS increased simultaneously and the upward trend of both peaks remained highly consistent with each other at the arousing stage. It is worth noting that when FAP reached and maintained at its upper limit (active status), the peaks of SEPS outputs presented coinstantaneous tiny fluctuations along with systolic FAP (arrows), implying an excellent sensitivity of the device in response to subtle changes of endocardial pressure even at a very high level.

The enlarged drawing of signals at the resting status is displayed in Figure 4d. Blood filling and subsequent ventricular contraction led to periodical but sudden changes of LVP, actuating contact and separation between the triboelectric layers of the SEPS and generating a significant voltage increase from 17.6 to 78.6 mV. Meanwhile, the diastolic and systolic pressures of femoral artery were 60.8 and 80.9 mmHg, respectively. The rising points of SEPS were highly synchronous to corresponding QRS complexes in ECG, which were widely perceived as signs of ventricular depolarization and the beginning of systole. The SEPS outputs arrived at the top just before aortic valves opening and blood pumping out from the heart, while the peak of FAP wave appeared when blood flow reached the commercial sensor placed in femoral artery, resulting in a period of leading time (LT = 174 ms) between two corresponding peaks. Therefore, the average velocity of blood flow can be calculated (Figure S4, Supporting Information).

By ruling out the influence of peripheral arteries on blood pressure which usually involved a chronic episode, both FAP and LVP depended upon the contractility of left ventricle, which enabled us to select FAP as a reference standard to evaluate the sensory functionality of the device. The climbing tendencies of both FAP and SEPS outputs during arousing stage were enlarged and contiguously depicted in an overlapping manner in Figure 4e, which further intuitively indicated the excellent consistency between the two signals. To quantitatively examine the consistency, a remarkable linearity (R^2 = 0.974) between the peaks of SEPS voltage and FAP was obtained (Figure 4f), which also significantly surpassed the previous work.[9] Based on the in vitro simulation results, the LVP can be calculated by the following formula

$$P\left(\mathrm{mmHg}\right) = 1.195\,U\left(\mathrm{mV}\right) \tag{2}$$

Therefore, the SEPS-derived systolic pressure inside left ventricular (P_{LVP}) was documented and compared with the extracted systolic FAP. As shown in Figure 4g, the dynamically changing systolic LVP measured by SEPS almost completely kept pace with the systolic FAP controlled by epinephrine, demonstrating the feasibility and stability of SEPS as an endocardial pressure self-powered sensor.

The left atrium is one of the four chambers of the heart, located on the left posterior side. Its primary roles are acting as a holding chamber for oxygenated blood returning from lungs and a pump to transport blood to left ventricle. Structural and functional heart diseases, such as atrial septal defect and heart failure, might lead to abnormal left atrial pressure (LAP).[16] LAP is a key hemodynamic index and could be quite meaningful for evaluating indications and contraindications of medical or surgical intervention for cardiovascular diseases and alarming some emergent circumstances, e.g., severe myocardial infarction accompanied by mitral valve prolapse.[17] However, currently there is a lack of widely accepted techniques for continuous and accurate LAP monitoring. Besides, LAP changes are relatively small, which puts forward a challenge for the sensitivity of the monitor device.

To validate the in vivo monitoring capability of LAP, the SEPS was implanted into the left atrium with an arterial pressure catheter placed in the left femoral artery, as schematically shown in **Figure 5**a and Video S3 (Supporting Information). The voltage outputs were collected while the heart contracted and relaxed (Figure 5b). At the heart rate of 114 bpm and the FAP of 92/70 mmHg, the maximal V_{oc} of the implanted SEPS was about 8 mV (6.9 mmHg). It is noteworthy that the variations of the V_{oc} signal were entirely synchronous to those of both the FAP and ECG signals. Interestingly, we found a tiny notch at the top of each V_{oc} waveform of the SEPS (red arrows). The notches occurred at the time points of the end of corresponding P waves (purple arrows) in ECG, which represented completion of depolarization and the beginning of left atrial contraction. The atrium contracts before the end of ventricular diastole to pump residual blood in atrium through atrioventricular valves, accompanied by a slight increase of LAP, which was successfully detected by the implanted SEPS. The results further proved that the device maintained its outstanding sensitivity at a pretty low level of pressure in left atrium.

Next, the in vivo output voltages obtained by the device under different levels of LAP were investigated. Acute and chronic heart failures involved deficiency of ventricular function share the common pathway of elevated LAP.[18] Application of cardiotonic agents such as epinephrine can reinforce ventricular contractility and accelerate ventricular emptying, thus reducing both the amount and time of blood filling in the left atrium, which leads to LAP decrease. As shown in Figure 5c, the femoral artery systolic pressure rose from 110 to 176 mmHg after injection of epinephrine. Consistently with the physiological principle, the peaks of V_{oc} decreased from 8 to 5.5 mV slowly, this opposite and descending tendency was synchronously to FAP, which can serve as an indicator of epinephrine potency.

Arrhythmias contribute to most of sudden cardiac deaths, which are constantly accompanied by abrupt influences on endocardial pressure due to abnormal electrical impulses among cardiomyocytes and hemodynamic disturbance inside heart's chambers. Therefore, we explored the feasibility of detecting arrhythmias by using the SEPS to monitor LVP changes. Ventricular premature contraction (VPC) was induced by stimulating the epicardium of ventricles with an external temporary pacemaker (Figure 5d). It is worth noting that an evidently increase of V_{oc} was observed, which was temporally corresponded to the ectopic R wave in ECG (the shaded area). The result indicated the occurrence of VPC. This phenomenon can be explained by the fact that advanced ventricular contraction brought forward the closure of mitral valves and impeded atrial

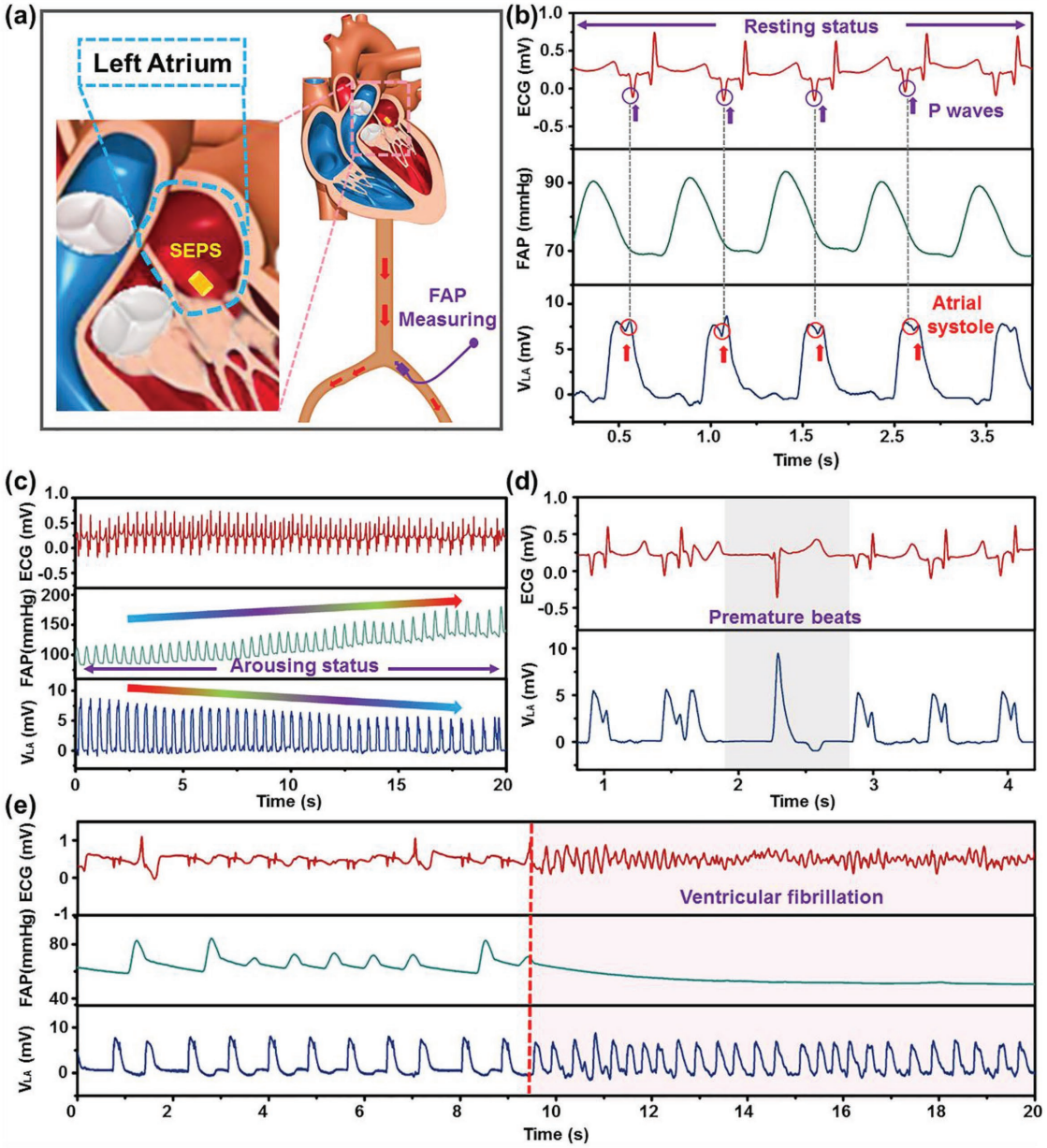

Figure 5. a) Schematic diagram of the SEPS implanted into left atrium and a commercial arterial pressure sensor placed in the right femoral artery. b) Detailed inspection into the corresponding relationship between waveforms of ECG and the SEPS outputs. c) The comparison among signals of ECG, FAP, and SEPS during reinforcing process of cardiac function. d) Ectopic R waves in representative ECG indicating ventricular premature contraction corresponded to enhanced waveform of the device. e) Disorganized waveforms of SEPS signals with quickened frequency were observed when ventricular fibrillation occurred.

emptying, which increased the blood volume in left atrium and subsequently elevated the LAP. Ventricular fibrillation (VF) is the most emergent and life-threatening arrhythmia. When VF occurred, the initial regular waveforms of SEPS outputs turned to be entirely disorganized in terms of rhythm and amplitude, with frequency markedly quickened (Figure 5e). Collectively, above results suggested that the output performance of the SEPS was closely associated with hemodynamic coordination and the level of endocardial pressure, which exhibits great potentiality in alerting fatal arrhythmias.

3. Conclusion

In summary, we developed a SEPS with significant advantages of miniature, high flexibility and ultrasensitivity to detect EP, which can be used to monitor vital signs of cardiovascular system. The miniaturization and flexibility of SEPS can reduce potential damage of implantation on heart tissue, leading to its broad applicability based on minimally invasive techniques. The long-term reliability and excellent blood compatibility of SEPS also meet the requirements of practical applications

of implantable medical sensors in human bodies. With the robust self-powered capability, the SEPS exempts the necessity of onboard battery. The EP inside heart chambers with a wide fluctuation range can be precisely monitored in real time with simple data processing. Besides, life-threatening arrhythmias can be also detected in a timely fashion based on sudden changes of EP. The proposed SEPS may promote the development of next-generation implantable biomedical sensor for monitoring and diagnosis of cardiovascular diseases.

4. Experimental Section

Fabrication of the SEPS: Nanostructured PTFE (50 μm) was employed as triboelectric layers. The nano-PTFE was formed by ICP with the etching gas of Ar, O_2, and CF_4. The steps corona discharge of nanostructured PTFE were described in a recent study by Shao et al.[14] Au film (100 nm) was deposited on the back of nano-PTFE by magnetron sputter as electrode, the nano-PTFE film was adhered to a Kapton substrate. Al foil (100 μm) served as both another triboelectric layer and the other electrode. Two package groups were involved in the encapsulation process of the SEPS: the first package group is PTFE layer (50 μm). Commercial PTFE was used without further treatment. Then PDMS mixed with specific ratio of curing agent were spin-coated on the device as the second package layer.

Hemolysis: The encapsulation layer samples and 10 mL saline were immersed into a silylation tube as the experimental group. Saline and distilled water with the same volume were utilized as the negative and positive control group, respectively. The SD rat blood (blood: sodium citrate = 4:1) was added to each group. After reacting in a water bath at 37 °C for 30 min, the supernatants were obtained using centrifuging process with 2500 revolutions per minute. The degree of hemolysis was determined spectrophotometrically by the concentration of hemoglobin in the supernatant at 545 nm. The formula for calculating the haemolysis rate is shown as follows

$$U_\eta = \frac{D_e - D_n}{D_p - D_n} \times 100\% \quad (3)$$

where, U_η is the hemolysis rate (%), D_e is the absorbance in the experimental group, D_n is the absorbance in the negative control group, and D_p is the absorbance in the positive control group. The value of $U_\eta \leq 5\%$ is taken as normal.

RBC Morphologies: After incubation with a bulk encapsulation layers in isotonic saline for 1 h at 4 °C, RBCs were collected and incubated in electron microscopy grade glutaraldehyde (2.5%) for 18 h. The cells were isolated by centrifugation (2500 rpm for 10 min) at room temperature and the supernatant was discarded. After washed once with saline, the fixed cells were then resuspended in 60% ethanol solution by gentle aspiration. The dehydration process was then proceeded by sequentially increasing quantities of ethanol (70%, 85%, 95%, and 100% v/v ethanol) before final recovery of the RBC pellet by centrifugation. RBCs were resuspended in absolute ethanol and dropped onto silicon wafer. After the evaporation of ethanol, gold deposition was performed for 30 s at 20 μA and examined by SEM.

In Vitro Platelet Adhesion Testing: Blood was obtained from SD rats. The whole blood was treated with the anticoagulant (sodium citrate). After centrifuging, the platelets and red blood cells were separated, and platelet rich plasma (PRP) was obtained. The samples were immersed in PRP and incubated at 37 °C for 2 h. The samples were subsequently rinsed with PBS solution to remove weakly adherent platelets. The adhered platelets were fixed with immunohistochemically fixed fluid (Beyotime) at room temperature for 12 h and rinsed three times with prewarmed PBS, and then dehydrated in a graded ethanol series, and critical point dried, and covered using a sputter coater with a layer of gold. Platelet morphology on the encapsulation layer was taken by SEM.

Animal Experiments: The procedures in handling the animals were strictly conformed to the "Shanghai Administration Rule of Laboratory Animal" and the Institutional Animal Care and Use Committee (IACUC) approved protocol of the Animal Care Center at the Second Military Medical University. Briefly, the animal was anesthetized with an injection of ketamine (8 mg kg^{-1}, intramuscularly (IM)) followed by propofol (1 mg kg^{-1}, intravenously (IV)) and then intratracheally intubated and ventilated in a rate of 5 s per cycle. Epinephrine (0.1 mg mL^{-1}, IV) was administered as the α-receptor agonist to increase the heart rate to simulate the active status. The devices were implanted in each swine's heart through surgery. In consideration of the miniaturized size (1 cm × 0.5 cm × 0.1 cm) and flexibility of the sensor, minimally invasive techniques with transapical access were utilized in the surgeries. Specifically, a ≈2 cm left anterolateral minithoracotomy in the sixth intercostal space was made to gain the access to the left ventricular apex. After opening the pericardium, two purse-string sutures (Prolene 2-0) were placed at the left ventricular myocardium with no apparent coronary arteries. The apex was then punctured, followed by insertion of the sheath of the SEPS transcatheter delivery system. After the SEPS was delivered to the desired heart chambers, the sheath was retracted, with the purse-string sutures tightened, which can stop bleeding and also fix the device. The more detailed experimental process are shown in Figure S5 (Supporting Information).

An arterial pressure catheter was placed in the right femoral artery and connected to the DAQ system (PowerLab 4/35). Probes fixed on the skin of the swine were connected to the DAQ system to record ECG results.

Characterization Methods: The open-circuit voltage, short-circuit current, and transferred charge were measured by an electrometer (Keithley 6517B) and recorded by oscilloscope (Teledyne LeCroy HD 4096) or DAQ system. The fabricated nanostructured PTFE film was processed by inductively coupled plasma (500, SENTECH/SI). The Au electrode was deposited by magnetron sputter (635, Denton Discovery). All SEM images were taken by Hitachi field emission scanning electron microscope (SU8020, HITACHI). All AFM images were taken by Asylum Research MFP-3D-SA-DV.

Supporting Information

Supporting Information is available from the Wiley Online Library or from the author.

Acknowledgements

Z.L., Y.M., H.O., and B.S. contributed equally to this work. The authors thank Dr. W. Jiang for his assistance with part of SEM observation. The authors also thank Dr. H. T. Yuan (BINN of CAS) for assistance in inductively coupled plasma etching system. The authors thank the support of National Key R&D project from Minister of Science and Technology, China (Nos. 2016YFA0202703, 2016YFC1101100, and 2016YFC1102202), National Natural Science Foundation of China (Nos. 61875015, 31571006, 11421202, 81601629, 61501039, 81800443, and 21801019), Beijing Talents Fund (No. 2015000021223ZK21), the Beijing Natural Science Foundation (Nos. 2182091 and 2162017), and the National Youth Talent Support Program. Z.L., Z.L.., H.Z., Y.F., Z.L., and H.O. conceived the idea and designed the experiments. Z.L., H.O., B.S., and D.J. designed and fabricated the SEPS. Z.L., H.O., B.S., and Y.Z. designed a model of the pressure change simulation experiment in vitro. Z.L., P.C., C.C., M.Y., and H.L. performed the cell culture study and studied the blood compatibility of the encapsulation layers. H.Z., Y.M., Z.L., H.O., N.L., F.X., D.Q., and Y.H. performed animal experiments. Z.L., H.O., and B.S. prepared figures and analyzed data. Z.L. and Y.M. wrote the manuscript, and all authors reviewed and commented on the manuscript. All authors have given approval to the final version of the manuscript. The grant number for the fund received from the National Key R&D project was corrected on January 15, 2019 after initial online publication.

Conflict of Interest

The authors declare no conflict of interest.

Keywords

cardiovascular disease, endocardial pressure sensor, minimally invasive, self-powered, triboelectric nanogenerator

Received: October 26, 2018
Published online: November 23, 2018

[1] C. M. Group, *N. Engl. J. Med.* **1991**, *325*, 293.
[2] R. Angie, J. M. Addington-Hall, A. S. M. Mccoy, P. M. Edmonds, A. J. Abery, A. J. S. Coats, J. Simon, R. Gibbs, *Eur. J. Heart Failure* **2014**, *4*, 283.
[3] V. C. Babaliaros, J. T. Green, S. Lerakis, M. Lloyd, P. C. Block, *J. Am. Col. Cardiol.* **2008**, *51*, 2116.
[4] B. Brochway, G. Doten (CROMPTON, SEAGER & TUFTE, LLC), *US 2002/0120200 A1*, **2002**.
[5] a) D. Khodagholy, T. Doublet, P. Quilichini, M. Gurfinkel, P. Leleux, A. Ghestem, E. Ismailova, T. Hervé, S. Sanaur, C. Bernard, *Nat. Commun.* **2013**, *4*, 1575; b) J. Rivnay, P. Leleux, M. Ferro, M. Sessolo, A. Williamson, D. A. Koutsouras, D. Khodagholy, M. Ramuz, X. Strakosas, R. M. Owens, *Sci. Adv.* **2015**, *1*, e1400251; c) R. Jonathan, I. Sahika, B. A. Collins, S. Michele, S. Eleni, S. Xenofon, T. Christopher, D. M. Delongchamp, G. G. Malliaras, *Nat. Commun.* **2016**, *7*, 11287; d) B. Shi, Z. Li, Y. Fan, *Adv. Mater.* **2018**, *30*, 1801511.
[6] a) Z. L. Wang, J. Song, *Science* **2006**, *312*, 242; b) F. R. Fan, Z. Q. Tian, Z. L. Wang, *Nano Energy* **2012**, *1*, 328; c) S. S. Kwak, H. Kim, W. Seung, J. Kim, R. Hinchet, S. W. Kim, *ACS Nano* **2017**, *11*, 10733; d) Z. L. Wang, *Mater. Today* **2017**, *20*, 74.
[7] a) Z. Li, G. Zhu, R. Yang, A. C. Wang, Z. L. Wang, *Adv. Mater.* **2010**, *22*, 2534; b) Q. Zheng, B. Shi, F. Fan, X. Wang, L. Yan, W. Yuan, S. Wang, H. Liu, Z. Li, Z. L. Wang, *Adv. Mater.* **2014**, *26*, 5851; c) M. Yuan, L. Cheng, Q. Xu, W. Wu, S. Bai, L. Gu, Z. Wang, J. Lu, H. Li, Y. Qin, *Adv. Mater.* **2014**, *26*, 7432; d) X. Yu, H. Wang, X. Ning, R. Sun, H. Albadawi, M. Salomao, A. C. Silva, Y. Yu, L. Tian, A. Koh, *Nat. Biomed. Eng.* **2018**, *2*, 165.
[8] W. Jiang, H. Li, Z. Liu, Z. Li, J. Tian, B. Shi, Y. Zou, H. Ouyang, C. Zhao, L. Zhao, R. Sun, H. Zheng, Y. Fan, Z. L. Wang, Z. Li, *Adv. Mater.* **2018**, *30*, 1801895.
[9] a) Y. Ma, Q. Zheng, Y. Liu, B. Shi, X. Xue, W. Ji, Z. Liu, Y. Jin, Y. Zou, Z. An, *Nano Lett.* **2016**, *16*, 6042; b) Q. Zheng, H. Zhang, B. Shi, X. Xue, Z. Liu, Y. Jin, Y. Ma, Y. Zou, X. Wang, Z. An, *ACS Nano* **2016**, *10*, 6510; c) C. Dagdeviren, F. Javid, P. Joe, T. v. Erlach, T. Bensel, Z. Wei, S. Saxton, C. Cleveland, L. Booth, S. McDonnell, J. Collins, A. Hayward, R. Langer, G. Traverso, *Nat. Biomed. Eng.* **2017**, *1*, 807; d) H. Ouyang, J. Tian, G. Sun, Y. Zou, Z. Liu, H. Li, L. Zhao, B. Shi, Y. Fan, Y. Fan, *Adv. Mater.* **2017**, *29*, 1703456.
[10] X. Cheng, X. Xue, Y. Ma, M. Han, W. Zhang, Z. Xu, H. Zhang, H. Zhang, *Nano Energy* **2016**, *22*, 453.
[11] a) D. Y. Park, D. J. Joe, D. H. Kim, H. Park, J. H. Han, C. K. Jeong, H. Park, J. G. Park, B. Joung, K. J. Lee, *Adv. Mater.* **2017**, *29*, 1702308; b) H. K. Dong, J. S. Hong, H. Lee, K. J. Chang, H. Park, G. T. Hwang, H. Y. Lee, D. J. Joe, J. H. Han, S. H. Lee, *Adv. Funct. Mater.* **2017**, *27*, 1606619; c) R. Hinchet, S. W. Kim, *ACS Nano* **2015**, *9*, 7742; d) Q. Zheng, Y. Zou, Y. Zhang, Z. Liu, B. Shi, X. Wang, Y. Jin, H. Ouyang, Z. Li, Z. L. Wang, *Sci. Adv.* **2016**, *2*, e1501478.
[12] a) Z. Bao, X. Chen, *Adv. Mater.* **2016**, *28*, 4177; b) W. Li, D. Torres, R. Díaz, Z. Wang, C. Wu, C. Wang, W. Z. Lin, N. Sepúlveda, *Nat. Commun.* **2017**, *8*, 15310; c) Y. Fang, X. Wang, S. Niu, S. Li, Y. Yin, K. Dai, G. Zhang, L. Lin, Z. Wen, H. Guo, *Sci. Adv.* **2016**, *2*, e1501624; d) P. K. Yang, L. Lin, F. Yi, X. Li, K. C. Pradel, Y. Zi, C. I. Wu, J. H. He, Y. Zhang, Z. L. Wang, *Adv. Mater.* **2015**, *27*, 3817.
[13] Q. Zheng, Y. Jin, Z. Liu, H. Ouyang, H. Li, B. Shi, W. Jiang, H. Zhang, Z. Li, Z. L. Wang, *ACS Appl. Mater. Interfaces* **2016**, *8*, 26697.
[14] J. J. Shao, W. Tang, T. Jiang, X. Y. Chen, L. Xu, B. D. Chen, T. Zhou, C. R. Deng, Z. L. Wang, *Nanoscale* **2017**, *9*, 9668.
[15] P. D. Stein, M. Marzilli, H. N. Sabbah, T. Lee, *Am. J. Physiol.* **1980**, *238*, H625.
[16] M. S. Maurer, P. B. Adamson, M. R. Costanzo, N. Eigler, J. Gilbert, M. R. Gold, M. Klapholz, L. A. Saxon, J. P. Singh, R. Troughton, *J. Card. Failure* **2015**, *21*, 479.
[17] W. T. Abraham, L. Perl, *J. Am. Coll. Cardiol.* **2017**, *70*, 389.
[18] J. Ritzema, I. C. Melton, A. M. Richards, I. G. Crozier, C. Frampton, R. N. Doughty, J. Whiting, S. Kar, N. Eigler, H. Krum, W. T. Abraham, R. W. Troughton, *Circulation* **2007**, *116*, 2952.